Model Predictive Control on a Fully-actuated Octocopter for Wind Disturbance Rejection

Caleb Probine, David Yang, Karl A. Stol*, and Nicholas Kay
University of Auckland, Department of Mechanical and Mechatronics Engineering, Auckland 1010, New Zealand

ABSTRACT

Physical interaction with the outdoors is a key application of UAVs. However, in these situations aircraft must compensate for external disturbances such as wind. Fully-actuated UAVs are well suited to this, but consideration is needed in control design. This work focuses on how Model Predictive Control (MPC) can be applied here. MPC has the advantage of being able to take system constraints into account, and its utility is investigated in wind rejection tasks. This work has focused on the formulation of appropriate constraints on craft-orientation and motor efforts. Also incorporated are frequency dependent actuator weightings, and basic disturbance estimation. Overall, in simulation, modelling of motor constraints was not found to be effective when compared to prior controllers. However, the use of MPC with angle constraints was found to improve position regulation. The controller was then verified with wind tunnel experiments.

1 INTRODUCTION

In recent years, Unmanned Aerial Vehicles (UAVs) have rapidly increased in their civil applications [1]. Examples of use cases include agriculture [2] or medical device supply [3]. This work in particular focuses on multirotor UAVs, which are advantageous for their agility and vertical takeoff ability. Furthermore, unlike fixed-wing UAVs, they can hold a position, which allows for physical interaction with the environment. This interaction has a range of implications, and it allows the use of UAVs in scenarios such as canopy sampling [4]. However, one major concern in these tasks is wind disturbances. Not only do winds have a mean component to resist, but also, unpredictable stochastic components.

One method by which rejection of these stochastic components can be eased is by using fully-actuated UAVs. Fully-actuated UAVs can produce forces and torques in any direction, and as such, translation and rotation of the aircraft are decoupled. This contrasts more conventional quadrotors, which must tilt to translate. Tilting is limited by the rotational inertia of the aircraft, which limits the bandwidth of this actuation. Meanwhile, fully-actuated UAVs and their ability to directly generate lateral forces, have significantly higher actuation bandwidths, making disturbance rejection easier. One type of fully-actuated drone is the fixed-tilt UAV, on which rotors are canted at constant angles. An example is shown in Figure 1, and this work will focus on these fixed-tilt UAVs.

A range of authors have already developed wind disturbance rejection for fully-actuated UAVs, and one example is the work in [6]. This describes a robust adaptive controller for a fully actuated octocopter similar to that shown in Figure 1. To account for disturbances, force-torque disturbances are estimated and used for regulation. The controller is then validated in simulation with a 'gust function'. While the controller shows good regulation ability, there are some limitations in the methodology. Firstly it is unclear whether the 'gust function' is backed up by literature. Furthermore, there are no experiments. However, these limitations are not unique to this work. The authors of [7] implement active disturbance rejection control on a passively-tilted craft, and similarly, they focus on simulation, using simple functions to generate force histories representing 'wind shear' or 'wind blow'. Meanwhile, the authors of [8] explore the application of sliding mode control for a tilting-rotors quadcopter. In this case, CFD is used to estimate the worst case disturbances, which are in turn used in simulation. However, this work again lacks experiments, and furthermore, the CFD methodology is not presented. Finally, the authors of [9], have designed another sliding mode controller for a tilting-rotors quadcopter. In the control design, torque disturbance effects are ignored, and a cuboid is used for the aerodynamic models. However, the use of mean wind, and Dryden turbulence models to generate wind profiles, does lend more validity. Nonetheless, experimental results are still not presented.

In the aforementioned work, a trend can be seen in fully-actuated UAV literature to only use simulation for the testing of wind rejection, with varying vigor. However, experimen-

Figure 1: Fixed-tilt Octocopter, utilised in [5]

*Email address: k.stol@auckland.ac.nz

tal validation is obviously of high importance. One work that provides this is [5]. Its author has designed an $\mathcal{H}_\infty$ controller for wind rejection on a fully-actuated octocopter. Experimental testing is then carried out in a wind tunnel to validate the controller's station keeping performance and shows improvements when compared to more traditional cascaded PID controllers. This work is not without issues though. One example, is that in simulation, some scenarios required re-tuning of the controller to avoid saturation of motor Pulse Width Modulations (PWMs). In the literature, there do exist other methods of experimental wind disturbance testing. For example, the authors of [10] fly aircraft outside. However, methods such as this, are limited by their repeatability. Meanwhile, the authors of [11] develop Iterative Learning Control for a fully-actuated craft and use air blowers to generate wind disturbances. However, in this case, details aren't present regarding wind affected area, or turbulence qualities. Across the works that have developed wind-rejecting controllers for fully-actuated UAVs, it is worth noting that none of them have explicitly dealt with the problem of saturation or constraints.

To handle the issue of constraints, one possibility is Model Predictive Control (MPC). MPC is an established control method, which relies on online optimisation. At each time step, a discrete plant model is used to gauge the response of the system to inputs. These control inputs are then chosen to minimise a cost function, and optimise future performance.

One of the critical advantages of MPC, is its ability to handle constraints, by incorporating them into the optimisation problem. This has been used on fully-actuated crafts in various works. The work in [12] constrains the forces and torques that the UAV produces in order to model the craft-limits. However this is possibly problematic in that the limits of each motor under combinations of forces may not be properly represented. The work in [13] provides an alternative solution to the actuator saturation problem. The authors of [13] discuss the fact that MPC applications on multirotors often apply a cascade control structure, with an unconstrained attitude controller. In these works constraints are then placed on state variables such as velocity or acceleration. Rather, in [13] a single monolithic Model Predictive Controller is used to control motors individually. Constraints are then applied to propeller rates for each rotor. A similar technique is utilised in [14] with constraints on propeller velocities. However, state constraints can still be valuable when, for example, obstacles need to be avoided in a trajectory, as shown in [15].

MPC can also be adapted to compensate for disturbances, via a range of techniques, some examples of which are given here. A common method, is the addition of control components for disturbance estimation. In [16], a wind disturbance is modelled as being driven by normally distributed noise. The disturbance is then estimated by an Extended Kalman Filter (EKF), and provided to the Model Predictive Controller. A similar approach is also taken in [12], where an EKF is used to compensate for disturbances and model uncertainty. Techniques other than Extended Kalman Filtering have also been used in works such as [17], where an Extended State Observer is used. One interesting point in [17], is that integral components are also incorporated into the Model Predictive Controller to reject slow moving disturbances. Finally, works such as [18], represent a more holistic incorporation of disturbances. In [18], robust MPC is used, in which, the optimisation is modified to minimise the cost, while considering the worst case disturbances. However, methods such as this can be overly conservative and complicated.

Overall, the work in [5] provides a strong basis for the continuation of wind rejection experiments for fully-actuated UAVs. However, constraints, such as motor saturation, remain an area to be explored. The literature has provided a range of methods to handle constraints with MPC. The main contribution of this paper is the implementation and experimental testing of a Model Predictive Controller on a fixed-tilt UAV, under wind disturbances. This facilitates investigation of the ability of MPC to improve constrained performance.

2 MODELLING

The UAV utilised is shown in Figure 1. It has a flying mass of $1.72\,kg$ and a rotor-to-rotor diameter of $500\,mm$. It is technically over-actuated due to its 8 rotors, but the focus in this work is on the features coming from full-actuation.

2.1 Co-ordinate Systems

Shown in Figure 2, a reference frame attached to the UAV-body is denoted by ${}^{\mathcal{B}}\bullet$. Positive ${}^{\mathcal{B}}[x, y, z]^\top$ denote the front, right and down directions respectively. Meanwhile ${}^{\mathcal{W}}\bullet$ defines the inertial frame in which the UAV's position can be perceived. For the wind, the simplifying assumption is also made that the dominant component is in the ${}^{\mathcal{W}}x$ direction.

2.2 Octocopter Dynamics

As discussed earlier, there are two ways of actuating this craft. *Attitude-based thrusts* arise due the horizontal force produced when the UAV is tilted. The desired components of the net vector, are denoted as ${}^{\mathcal{W}}F_A$, and this is produced by manipulating roll ψ and pitch θ. The unique translational forces that an Octocopter can generate are then discussed as *Vectored thrust* (${}^{\mathcal{B}}F_{V,x,y}$). In this case, rotors are selectively sped up to generate a net horizontal force. Given the higher bandwidth, it is desired to use vectored thrust to reject high frequency wind components. Meanwhile, attitude-based thrust should ideally be used to reject other components of the wind, given its better efficiency. These actuation methods are shown in Figure 2. Because attitude-based thrust is to be used for low frequency wind components, and mean wind is assumed to exist in the ${}^{\mathcal{W}}x$ axis alone, roll control will be ignored in this work. Rather, any ${}^{\mathcal{W}}y$ regulation will be done with ${}^{\mathcal{B}}F_{V,y}$. This work also assumes ψ (yaw) deviation is negligible, such that the ${}^{\mathcal{B}}xz$ and ${}^{\mathcal{W}}xz$ planes are coincident throughout control. Note that this does not assume $\tau_z = 0$, but rather that the yaw regulation is perfect.

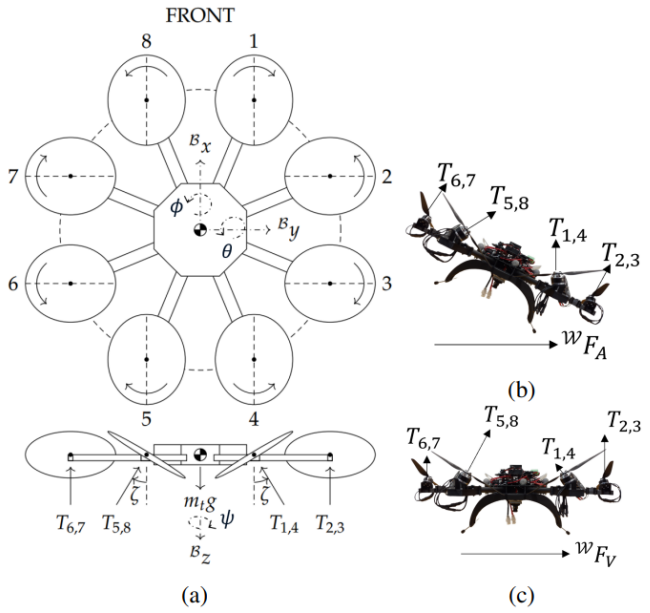

Figure 2: Craft dynamics illustrations. (a) Octocopter Schematic [5]; (b) Attitude-based thrust ${}^{\mathcal{W}}F_A$ in the ${}^{\mathcal{W}}y$ direction; (c) Vectored thrust ${}^{\mathcal{B}}F_V$ in the ${}^{\mathcal{B}}y$ direction

2.3 *Existing Control Architecture and Model Components*

The numerical model of the UAV is taken from [5], and includes a motor model, rigid body dynamics model and aerodynamic correlations. While detailed, limitations of this model include omitted dynamics, due to the empirical nature of the aerodynamic models, and unmodelled interactions between adjacent rotors due to cross flow. Alongside the physical components, the low-level control elements also need to be considered, as they are to be incorporated in the overall plant model that MPC uses. This includes the baseline attitude controller, as well as a motor mixer. Figure 3 then shows how all of these plant model components are combined.

This allows the designation of inputs for the model predictive controller to manipulate, as follows. The first two inputs are ${}^{\mathcal{W}}F_{A,x}$ and ${}^{\mathcal{W}}F_{A,z}$. Together these define the attitude-based thrust vector to be produced. They are converted to a single ${}^{\mathcal{B}}z$ thrust (the magnitude) and an angle setpoint θ. The Attitude Controller utilised here is the default from the PX4 flight stack, and it generates the torque vector for the aircraft. Vectored thrusts ${}^{\mathcal{B}}F_{V,x}$ and ${}^{\mathcal{B}}F_{V,y}$ are also directly manipulated by the model predictive controller. Manipulation in the body frame is used to ease the conversion of these values to motor efforts. The body to world frame conversion is then encoded via the linearisation, and any effects should be small near the operating point. From the torques and vectored thrusts supplied as commands to the UAV, the Multirotor Mixer then generates PWMs for each of the motors. For this craft, the mixer is simply a matrix $\mathcal{M} \in \mathbf{R}^{8\times 6}$

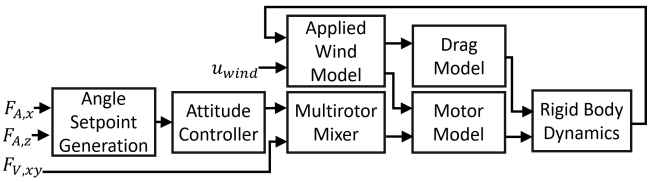

Figure 3: Model to be controlled by the Model Predictive Controller, developed in [5]

3 MODEL PREDICTIVE CONTROL FORMULATION

The aforementioned model is included in the controller as a discrete time state space model, for prediction. At each time step, a cost function is minimised, for the next N_p timesteps. To achieve this objective, the first N_c control actions are manipulated. When an optimal control sequence is determined, the first-time-step control action is applied to the plant. Constraints are then incorporated, by defining them as a linear inequality of inputs and outputs, with the format in Equation 1. In this equation $\mathbf{u}$ and $\mathbf{y}$ are input and outputs of the plant, $\mathbf{G}$ is a vector of constraint boundaries and E/F are matrices that encode the constraint coefficients.

$$E\mathbf{u} + F\mathbf{y} \leq \mathbf{G} \tag{1}$$

In MATLAB and Simulink, a suite of tools are used to setup the optimisation. As such this section details the formulation of appropriate architectures, constraints and models.

3.1 *Controller Architecture*

Mentioned earlier was the use of vectored and attitude-based thrusts at appropriate frequencies (Section 2.2). A potential method is the integration or filtering of a single control input to allocate between vectored and attitude-based thrust. However, the induced coupling between the thrusts would make constraint satisfaction difficult. Consequently, they were controlled independently. To add frequency dependent allocation, auxiliary states for the low-passed vectored thrust were added to the controller and weighted. This allowed for the penalisation of mean-value build-up in the vectored thrust. Meanwhile, the attitude-based thrust was controlled via an integral component. As such the output of the controller was $\frac{d}{dt}F_{A,x}$. By weighting the change in attitude-based thrust, high frequency components could effectively be penalised. This control architecture is shown in Figure 4.

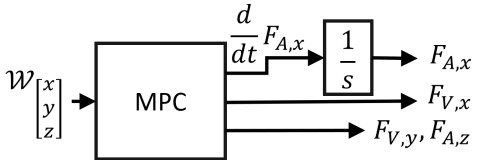

Figure 4: Model Predictive Controller Architecture

3.2 Constraints

3.2.1 Motor Constraints

The motivation for motor constraints arises in [5], in which, a range of different conditions necessitated re-tuning of the developed $\mathcal{H}_\infty$ to avoid violation. To formulate constraints, each motor was constrained individually, similar to [13]. However, in the case of this work, PWMs are constrained rather than propeller rates. This is because PWM saturation was highlighted in [5]. The core issue here was to determine how to appropriately constrain the PWMs, when they were not directly controlled. To do so, the motor map was used, allowing constraint formulation as shown in Equation 2. In Equation 2, the PWMs are on a normalised scale of $[0, 1]$.

$$\mathbf{0} \leq \mathcal{M} \begin{bmatrix} {}^{\mathcal{B}}C_\eta \\ {}^{\mathcal{B}}T \end{bmatrix} \leq \mathbf{1} \tag{2}$$

In this equation ${}^{\mathcal{B}}C_\eta$ and ${}^{\mathcal{B}}T$ are the vectors of torques and forces respectively, produced by the craft. However, not all forces and torques are generated by the Model Predictive Controller. The first two elements of ${}^{\mathcal{B}}T$, ($F_{V,x}$ and $F_{V,y}$) are manipulated directly by the controller. However, the other elements must be approximated or measured.

One assumption can be made with respect to roll and yaw. They have zero references, and so do not contribute to craft-translation. In fact, in simulation the roll and yaw angle values have standard deviations less than $0.2°$. As such, the roll and yaw torques are assumed not to significantly affect the remaining dynamics, and they are decoupled in the model. They are then simply measured by the Model Predictive Controller, and input to the constraints.

${}^{\mathcal{B}}T_z$ can also be easily approximated. This thrust is generated from $F_{A,z}$ and $F_{A,x}$, by a two-norm operation. This can simply be linearised about an operating point. Similarly, while the pitch torque is not generated by MPC, it is related to $F_{A,x}$, $F_{A,z}$ and the internal states of the attitude controller. As such, the pitch torque can be approximated from the estimates of the attitude controller states. The overall relationships are formulated in Equation 3.

$$\mathbf{0} \leq \begin{bmatrix} \mathcal{M}_{\tau_x}^\top \\ \mathcal{M}_{\tau_y}^\top \\ \mathcal{M}_{\tau_z}^\top \\ \mathcal{M}_{T_x}^\top \\ \mathcal{M}_{T_y}^\top \\ \mathcal{M}_{T_z}^\top \end{bmatrix}^\top \begin{bmatrix} \tau_x \\ c_1 F_{A,x} + c_2 F_{A,z} + \mathbf{C_1}\hat{\mathbf{x}}_{\mathbf{PID}} \\ \tau_z \\ F_{V,x} \\ F_{V,y} \\ c_3 F_{A,x} + c_4 F_{A,z} \end{bmatrix} \leq \mathbf{1} \tag{3}$$

In Equation 3, c_1, c_2, $\mathbf{C_1}$, c_3 and c_4 are linearisation constants. Also note that $F_{V,x}$ and $F_{V,y}$ are outputs of the controller, while τ_x and τ_z are measured. Finally, $\hat{\mathbf{x}}_{\mathbf{PID}}$ represents the internal state estimates for the attitude controller.

3.2.2 Angular Constraints

While not an initial concern in [5], another constraint considered was the aircraft orientation. An orientation limit may be motivated by a tool being used, or a requirement to keep a low vertical profile. As the wind is assumed to be coming from the $\mathcal{W}_x$ direction, the focus was on pitch constraints (θ).

This was considerably easier to incorporate into the control architecture, compared to PWM. The pitch angle was already a state in the model, and was constrained between two limits. The pitch angle setpoint was also constrained. Similar to the ${}^{\mathcal{B}}T_z$ thrust, the pitch setpoint was directly related to $F_{A,z}$ and $F_{A,x}$. This relationship was again linearised to generate the pitch set-points of the aircraft, and subsequently constrained. It is worth noting that these constraints were *soft*. This is because the controller was not necessarily able to directly manipulate θ, as it was a state variable, rather than a control input. The use of soft constraints defines a limit, with a significant cost being imposed if said limit is exceeded.

3.3 Linearisation and Model Generation

One requirement for the Model Predictive Controller generation was a linear model to predict from. From [5], a non-linear model model was already available. This had also been linearised in [5], but to account for new plant outputs, this was repeated. The linearisation point was found by trim analysis. This was carried out with an input wind speed of $\mathbf{u} = [5.6\ 0\ 0]\, m/s$, and with the constraint that attitude-based thrust was exclusively being used to reject this mean wind. The wind velocity was chosen for consistency with results in [5]. Edits were then made to include features such as the low passing of vectored thrust and decoupling of yaw and roll torque measurements from controller states. A minimal realisation was also taken to eliminate one state that did not effect the weighted or constrained dynamic behaviour.

3.4 Disturbance Estimation

In the MPC toolbox used, a Kalman Filter was generated automatically. This allowed estimation of unmeasured components such as the attitude controller's internal states. However, this tended to fail under non-zero-mean disturbances, including both deviations of the mean wind from $5.6m/s$, and biases in sensor measurements. To compensate, simple disturbance estimators were added. These were formulated as auxiliary plant model states, which were in turn estimated by the Kalman Filter. These auxiliary states were modelled as integrators, driven by gaussian noise, shown in Equation 4.

$$\dot{x}_{aux} = B w_d \tag{4}$$

For input disturbances, the estimated state, is then fed into the state space model as shown in Equation 5.

$$\dot{x} = Ax + Bu + B_d x_{aux} \tag{5}$$

Meanwhile, for output disturbances the auxiliary state is simply added to the respective output as a bias.

The wind is modelled as an input disturbance, and the B_d matrix maps how a change in wind speed from the equilibrium point impacts the plant. This matrix was found during linearisation, and it allows the controller to perceive the effects of mean wind deviations. Meanwhile, output disturbances were included on the measured pitch angle, and the world frame velocities, to improve state estimation quality. Under preliminary simulation, disturbance estimation was found to help prevent $\mathcal{W}_x$ steady state errors. In this sense, the disturbance estimator acted similarly to an integral component in the controller. However, it has the dual advantage of also improving state estimate accuracy overall.

3.5 Final Parameters

The sample time was chosen by comparing the Model Predictive Controller's computational requirements to a known significant load on the PX4 flight stack in simulation. This informed a sample rate choice of $10\,Hz$. To determine the control and prediction horizons, they were chosen by balancing performance (as measured by root mean square (RMS) position error) and the allowable computational load. This resulted in horizons of $N_c = 3$ and $N_p = 8$.

In testing, the baseline controller for testing is the $\mathcal{H}_\infty$ controller developed in [5]. As such, the Model Predictive Controller weights were tuned by running it, and the $\mathcal{H}_\infty$ controller under wind, and ensuring that the standard deviations of each actuation method: e.g. $F_{V,x}$ and $F_{A,x}$, were similar. The power spectral densities were also verified to ensure they were fairly similar in shape. The weights manipulated were those on velocity, vectored thrust, and attitude-based thrust-rate. The velocity weight was increased mainly due to perceived resonance issues during preliminary experimental implementations. Meanwhile, throughout tuning, changing the low pass portion of the weighting did not significantly affect frequency allocation, as the normal vectored thrust weight was sufficient to generate the required effect. The final parameters chosen are summarised in Table 1. Note that scale factors were also used to improve numerical conditioning.

x, y, z	$F_{V,x}$	$F_{V,y}$	$F_{A,z}$	$\dot{x}, \dot{y}, \dot{z}$	$\dot{F}_{A,x}$	F_{xlp}
1	6.66	4	3.3	1.2	0.06	0.1

Table 1: Model Predictive Controller weights

4 TESTING METHODOLOGY

4.1 Simulation Methodology

The simulation is based on the non-linear model described in Section 2, Also included for simulation is a sensor model, as well as input wind trajectories. The trajectories utilised are also taken from [5], and are comprised of generated turbulent wind data with a mean speed of $5.6m/s$. The turbulence intensities are 10.03%, 8.28% and 8.02% for the $\mathcal{W}_x$, $\mathcal{W}_y$ and $\mathcal{W}_z$ axes respectively. At the beginning of each simulation a 10s period is allowed for the wind to ramp up.

To test PWM constraints in simulation, actuator saturation was induced for each controller. For $\mathcal{H}_\infty$, saturation is induced between the mixer and motors (Their relative positions in simulation are as shown in Figure 3). Meanwhile, for MPC, the optimisation's perception of the constraints is instead tightened. Under different saturation levels, the simulation is run for 120s, and the data is inspected to determine if position diverges. To impose angle constraints with $\mathcal{H}_\infty$ the pitch component of the angle setpoint was saturated. For MPC, the angle limits were updated in the optimisation. With angle limits, position variation was used for comparison.

4.2 Experimental Methodology

To convert the Model Predictive Controller for use with the PX4 flight stack, Simulink code generation was used. This generated a C++ class, with methods to execute each control step. This class was then added to the flight stack as its own module. Using radio-controlled switches, the MPC and Default controllers could then be switched as appropriate. The flight hardware used was a Pixhawk 4 controller.

The experimental results themselves came from the closed loop wind tunnel shown in Figure 5. For UAV flight, this was equipped with a motion capture system to provide accurate position feedback. A turbulence grid was also installed in the tunnel, and induced time varying components in the flow. The turbulence intensities in each axis are 11.6%, 6.2% and 7.3% for the $\mathcal{W}_x$, $\mathcal{W}_y$ and $\mathcal{W}_z$ axes respectively.

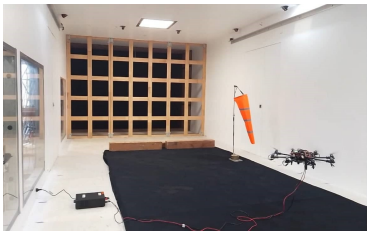

Figure 5: University of Auckland Closed Loop Wind Tunnel, with a turbulence grid and motion capture system.

5 RESULTS

5.1 Unconstrained Performance

5.1.1 Simulation

First tested was an unconstrained Model Predictive Controller. This was simulated for the purposes of verifying that actuator allocation was occurring as designed. Figure 6 shows the variation of attitude-based and vectored thrust based actions for the tuning described in section 3.5.

While it can be seen that attitude-based thrust is successfully used to compensate for mean wind, the vectored thrust seems to have less variation at all frequencies. This is due to the match to the actuator usage in [5]. However, a weight modification, shown in Figure 7, demonstrates that more appropriate actuator usage is possible. In this figure, vectored

thrust is shown to dominate at high frequencies. However, further experiments retain the matched tuning.

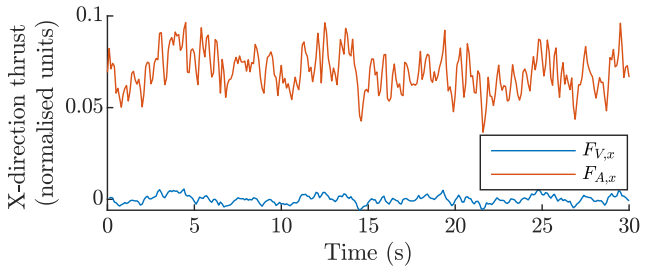

Figure 6: Simulation results of unconstrained MPC, showing the ${}^{\mathcal{W}}x$ vectored and attitude-based thrusts used

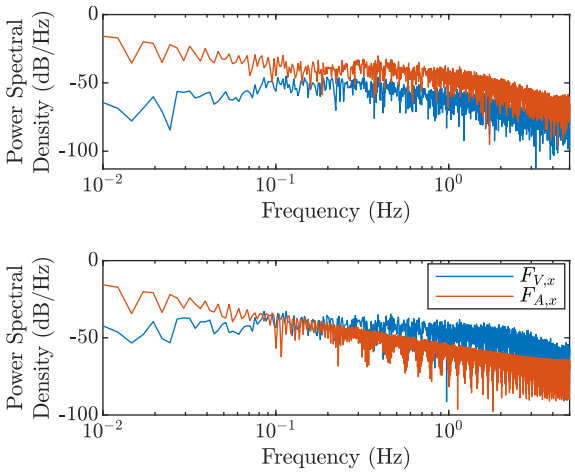

Figure 7: Actuator power spectral densities from simulation. The upper plot shows the frequency content for the default tuning. The lower plot shows the frequency content with more aggressive weights ($w_{F_{V,x}} = 0.666; w_{\dot{F}_{A,x}} = 1$)

5.1.2 Experiment

Figure 8 shows the $\mathcal{W}_x$ position trajectory for a 50s period. Overall, the mean is $-8mm$, and the standard deviation is $10mm$. In the other axes, performance is less strong, with the $\mathcal{W}_y$ and $\mathcal{W}_z$ mean values being -82, and $110mm$ respectively. However, this is easily explained by the fact that wind is only modelled in the $\mathcal{W}_x$ axis. As such disturbances or imbalances in other axes can not be accounted for. The standard deviations for these axes are still low, at $6mm$ and $7mm$ respectively. After removing the steady state errors the RMS position error was found to be $13mm$. This is comparable, to the $\mathcal{H}_\infty$ controller from [5], albeit slightly worse.

5.2 *Motor Constraint Testing*

The simulation stability of the controllers under different motor constraint conditions is shown in Table 2. Figure 9 then

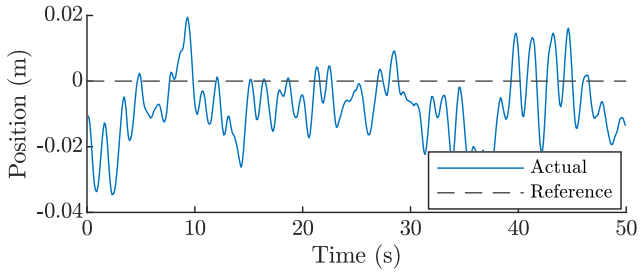

Figure 8: Experimental unconstrained MPC position tracking

shows the position trajectories of the $\mathcal{H}_\infty$ and Model Predictive Controllers for the test case [0.405 0.595]. Overall, the $\mathcal{H}_\infty$ controller appears to be slightly better at handling actuator saturation. This is counter-intuitive, but it is theorised to be related to the inherent redundancy provided by the craft's 8 rotors. When 4 rotors are saturated, the aircraft can often still maintain quadrotor-like control schemes. Meanwhile, the fact that the MPC destabilises earlier is suspected to be related to the approximate nature of constraints and the extensive linearisation use. The ultimate conclusion is that this cascade MPC architecture is insufficient for handling actuator limits.

Lower PWM Limit	Upper PWM Limit	$\mathcal{H}_\infty$ Stable	MPC Stable
0.4	0.6	Y	Y
0.405	0.595	Y	N
0.41	0.59	N	N
0.4	1	Y	Y
0.425	1	Y	N
0.430	1	N	N
0	0.54	Y	N
0	0.535	N	N

Table 2: Constrained simulation stability. Full range: [0 1]

5.3 *Angle Constraint Testing*

5.3.1 Simulation

From trim analysis, the required pitch angle for a 5.6m/s wind is $8°$. As such, the controllers are tested with a smaller limit of $6°$. The controller performance is shown in Figure 10, demonstrating that with MPC, the constraint is obeyed, with only occasional violations. Furthermore, the MPC shows far better regulation performance. The minor violations can be compensated for with a safety factor in the constraint.

5.3.2 Experimental Results

When angle is constrained to $6°$ under a wind of $5.6m/s$, the $\mathcal{W}_x$ axis results can be seen in Figure 11. In this case, performance is worse compared to Figure 8, with a steady state error of approximately -$58mm$. This is because, when under

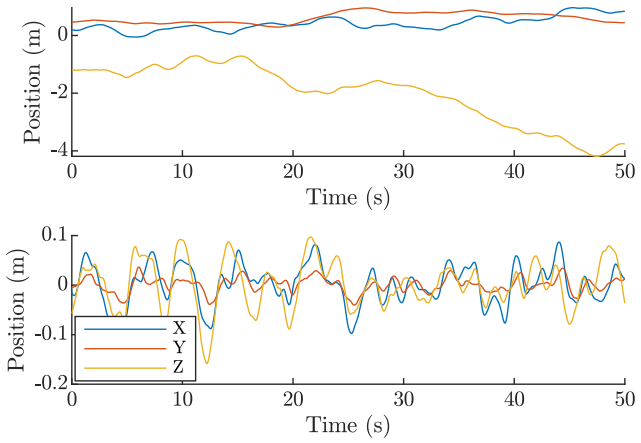

Figure 9: Simulation results of MPC (top) and $\mathcal{H}_\infty$ (bottom) position tracking with imposed constraints [0.405, 0.595]

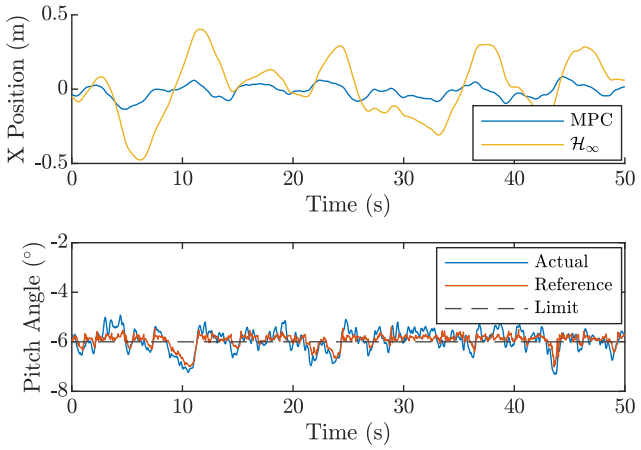

Figure 10: Simulation comparison of MPC and $\mathcal{H}_\infty$ under turbulent wind. Top: ${}^{\mathcal{W}}x$ position tracking; Bottom: pitch angle θ with a soft limit of 6° (MPC Only)

an angle constraint, vectored thrust is rejecting mean wind components, while also being weighted at low frequencies. However, this is still less than the performance degradation seen for $\mathcal{H}_\infty$ in simulation. Namely, while simulation and experiment cannot be compared directly, simulation showed that transient angle-constrained $\mathcal{H}_\infty$ performance was much worse than MPC (Figure 10). Translating this relative performance into experiment, it would be expected that the increased variance under $\mathcal{H}_\infty$ exceed the MPC steady-state error. In any case, this steady state error could also be fixed by position-integral weights. The standard deviation in the $\mathcal{W}_x$ axis is also increased compared to the unconstrained case, at $14mm$, but the change is slight. Finally, in the $\mathcal{W}_z$ axis, a $377mm$ steady state error, is introduced under an angle constraint. This is again suspected to be related to mean wind in this axis, and the fact that the UAV is operating at an angle below that of the linearisation point. As such, the mean vertical thrust required changes, which cannot fully be corrected by MPC, while staying at the origin. As above, this could be fixed with integral weights.

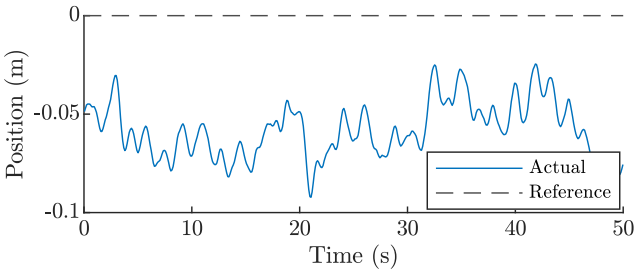

Figure 11: Experimental results of MPC position tracking

The angle constraint was also satisfied as shown in Figure 12. It shows that angle increases up to a limit, after which, ${}^{\mathcal{B}}F_{V,x}$ begins to vary more, and partially reject mean wind.

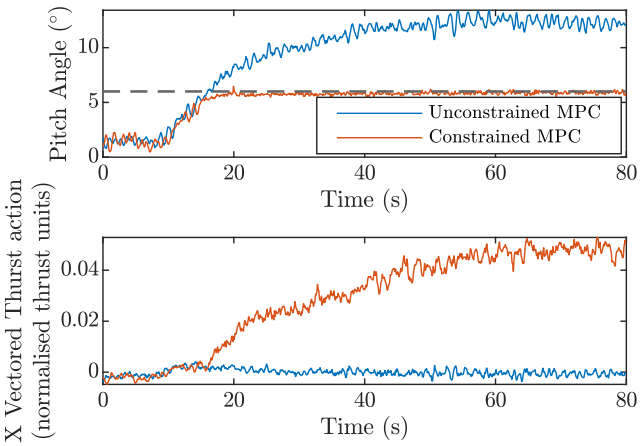

Figure 12: Experimental comparison of constrained and unconstrained MPC with turbulent wind. Top shows pitch angle regulation; bottom shows ${}^{\mathcal{B}}F_{V,x}$ (vectored thrust) usage

6 CONCLUSION

This work has presented the development of a Model Predictive Controller for a fully-actuated UAV under wind disturbances. The ability to handle wind is key for physical environmental interaction, and prior work has established a range of control methods to facilitate this. However, one concern that arose was constraint handling. MPC development for the constraint of motor efforts and orientations has been carried out. Other controller features are weightings that provide frequency-based actuator allocation, and disturbance estimators to handle deviations in the wind from the operating point.

In simulation, UAV motor effort constraints were found to be ineffective compared to the prior $\mathcal{H}_\infty$ controller. However, MPC usage for the constraint of angle showed promise. In

experiments, under an increasing wind, the Model Predictive Controller successfully restrained the angle to 6°.

Future work will more rigorously test the controller. In particular, variations in wind speeds and craft parameters need to be investigated. The controller could also be extended, for example, with angle constraints about more axes.

ACKNOWLEDGEMENTS

The research reported was conducted as part of "Enabling unmanned aerial vehicles (drones) to use tools in complex dynamic environments UOCX2104", funded by the New Zealand Ministry of Business, Innovation and Employment.

REFERENCES

[1] Hazim Shakhatreh, Ahmad H. Sawalmeh, Ala Al-Fuqaha, Zuochao Dou, Eyad Almaita, Issa Khalil, Noor Shamsiah Othman, Abdallah Khreishah, and Mohsen Guizani. Unmanned aerial vehicles (UAVs): a survey on civil applications and key research challenges. *IEEE Access*, 7:48572–48634, 2019.

[2] Victoria Gonzalez-Dugo, P. Zarco-Tejada, E. Nicolás, Pedro Antonio Nortes, J. J. Alarcón, Diego S. Intrigliolo, and E.J.P.A. Fereres. Using high resolution UAV thermal imagery to assess the variability in the water status of five fruit tree species within a commercial orchard. *Precision Agriculture*, 14(6):660–678, 2013.

[3] Charles T. Howell III, Frank Jones, Taylor Thorson, Richard Grube, Cecil Mellanson, Lee Joyce, John Coggin, and Jack Kennedy. The first government sanctioned delivery of medical supplies by remotely controlled unmanned aerial system (UAS). Technical report, NASA Langley Research Center, 2016.

[4] James R. Kutia, Karl A. Stol, and Weiliang Xu. Aerial manipulator interactions with trees for canopy sampling. *IEEE/ASME transactions on mechatronics*, 23(4):1740–1749, 2018.

[5] Jérémie Xavier Joseph Bannwarth. *Aerodynamic modelling and wind disturbance rejection of multirotor unmanned aerial vehicles*. PhD thesis, The University of Auckland, 2021.

[6] Panfeng Shu, Feng Li, Junjie Zhao, and Masahiro Oya. Robust adaptive control for a novel fully-actuated octocopter uav with wind disturbance. *Journal of Intelligent & Robotic Systems*, 103(6):1–17, 2021.

[7] Santos Miguel Orozco Soto, Jonathan Cacace, Fabio Ruggiero, and Vincenzo Lippiello. Active disturbance rejection control for the robust flight of a passively tilted hexarotor. *Drones*, 6(9):258, 2022.

[8] Siddharth Sridhar, Gaurang Gupta, Rumit Kumar, Manish Kumar, and Kelly Cohen. Tilt-rotor quadcopter xplored: hardware based dynamics, smart sliding mode controller, attitude hold & wind disturbance scenarios. In *American Control Conference (ACC)*, pages 2005–2010, 2019.

[9] Shilin Yi, Keigo Watanabe, and Isaku Nagai. Anti-disturbance control of a quadrotor manipulator with tiltable rotors based on integral sliding mode control. *Artificial Life and Robotics*, 26(4):513–522, 2021.

[10] Gerardo Flores, Andrés Montes de Oca, and Alejandro Flores. Robust nonlinear control for the fully actuated hexa-rotor: theory and experiments. *IEEE Control Systems Letters*, 7:277–282, 2022.

[11] Pengkang Yu. *An over-actuated multi-rotor aerial platform and iterative learning control applications*. PhD thesis, University of California, Los Angeles, 2022.

[12] Maximilian Brunner, Karen Bodie, Mina Kamel, Michael Pantic, Weixuan Zhang, Juan Nieto, and Roland Siegwart. Trajectory tracking nonlinear model predictive control for an overactuated MAV. In *IEEE International Conference on Robotics and Automation (ICRA)*, pages 5342–5348, 2020.

[13] Davide Bicego, Jacopo Mazzetto, Ruggero Carli, Marcello Farina, and Antonio Franchi. Nonlinear model predictive control with enhanced actuator model for multi-rotor aerial vehicles with generic designs. *Journal of Intelligent & Robotic Systems*, 100(3):1213–1247, 2020.

[14] Mohit Mehndiratta, Karanjot Singh, Erdal Kayacan, and Mir Feroskhan. Receding horizon-based fault-tolerant control of QuadPlus: an over-actuated quadrotor. In *IEEE 17th International Conference on Automation Science and Engineering (CASE)*, pages 853–859, 2021.

[15] Chuanbeibei Shi and Yushu Yu. Design and implementation of a fully-actuated integrated aerial platform based on geometric model predictive control. *Micromachines*, 13(11):1822, 2022.

[16] Kostas Alexis, George Nikolakopoulos, and Anthony Tzes. Switching model predictive attitude control for a quadrotor helicopter subject to atmospheric disturbances. *Control Engineering Practice*, 19(10):1195–1207, 2011.

[17] Tong Lv, Yanhua Yang, and Li Chai. Extended state observer based MPC for a quadrotor helicopter subject to wind disturbances. In *Chinese Control Conference (CCC)*, pages 8206–8211, 2019.

[18] Kostas Alexis, Christos Papachristos, Roland Siegwart, and Anthony Tzes. Robust model predictive flight control of unmanned rotorcrafts. *Journal of Intelligent & Robotic systems*, 81(3-4):443–469, 2015.